Materials Research. 2014; 17(5): 1302-1308
DOI: http://dx.doi.org/10.1590/1516-1439.285914

Study of Expanded Austenite Formed in Plasma Nitrided AISI 316L Samples, Using Synchrotron Radiation Diffraction

***Marcelo Campos*[a,b]*, *Sylvio Dionysio de Souza*[a,c], *Luis Gallego Martinez*[d], *Maristela Olzon- Dionysio*[a,c]**

[a]*Departamento de Física, Universidade Federal de São Carlos – UFSCar, São Carlos, SP, Brasil*
[b]*Embrapa Instrumentação, Empresa Brasileira de Pesquisa Agropecuária, São Carlos, SP, Brasil*
[c]*Instituto de Ciências e Tecnologia, Universidade Federal dos Vales do Jequitinhonha e Mucuri – UFVJM, Diamantina, MG, Brasil*
[d]*Centro de Ciência e Tecnologia de Materiais, Instituto de Pesquisas Energéticas e Nucleares – IPEN, São Paulo, SP, Brasil*

Received: April 7, 2014; Revised: October 9, 2014

AISI 316L stainless steel samples nitrided at different conditions of temperature and time, showing different properties, such as nitrogen concentration (C_N) and nitrided layer thickness, were studied. Expanded austenite (γ_N) diffraction peaks up to the (222) reflection were observed using suitable wavelength synchrotron radiation. XRD patterns were fitted by Le Bail method, using a special triclinic crystal structure (with a lattice distortion η) for γ_N, whose peaks were decomposed in a few subpeaks, to consider C_N gradient across the nitrided layer. Our results indicate that regarding γ_N magnetic behavior, which was observed for the samples nitrided at 450 °C, it seems to be correlated not only to high C_N (≥31at.%), but also to higher η (≥2.4°), which reaches up to 5.6°. This distortion η decreases when C_N increases, consequently, with its minimum close to the surface. On the other hand, for paramagnetic samples (350 °C), η increases up to 1.4° when C_N increases up to 30 at.%.

Keywords: *AISI 316L stainless steel, plasma nitriding, expanded austenite, layer depth, synchrotron diffraction, magnetic character*

1. Introduction

Plasma nitriding of stainless steels improves some of their tribological properties[1-5] as a result of the nitrided layer, which is formed on the surface, whose properties depend strongly on the conditions used in the process, such as gas composition and pressure, temperature and time. If the temperature is lower than 450 °C, an expanded austenite phase (γ_N), which presents a large nitrogen concentration, is formed. This layer shows higher hardness and higher pitting corrosion resistance in comparison with the untreated austenite (γ)[6-9].

Compared to γ reflections, γ_N peaks are broader and shifted to lower diffraction angles. The γ_N(200) positions are more deviated relatively to the γ(200) diffraction angle than the other planes, demonstrating a deviation from the cubic fcc unit cell. The structure of this phase is still a matter of controversy which has not yet been completely clarified[10-15]. Fewel et al.[10] employed both Cu-Kα and Co-Kα radiations to measure X-ray Diffraction (XRD) patterns up to the (420) reflection for *one* selected nitrided sample. They analyzed the XRD patterns trying different structures, like tetragonal, monoclinic and triclinic, obtaining the best agreement of their data for the latter one. Particularly, it is a structure which presents a low symmetry, but they used to represent it as a fcc structure with distortion. To do this, the lattice parameters are equal and a distortion ε (in this paper η will be used for this distortion, not to be confused with ε phase).

*e-mail: marcelobtu@gmail.com

This model was tested by Mingolo et al.[14], who used Cu-Kα to measure a lower number of reflections, up to (400). They studied the γ_N phase observed for the surface of *two* AISI 316L nitrided samples, describing it well by a triclinic structure, instead of tetragonal or monoclinic. In a more recent study of *seven* nitrided samples using synchrotron radiation diffraction, Fewell and Priest[15] observed peaks up to (622) reflection. In their study, they tested a total of ten plausible candidate structures in order to propose a structure for this phase. They examined in details *two* of the seven samples and concluded that none of the candidate structures work well at high order reflections and each presents its particular difficulties at a lower order. However, they affirm […] the triclinic lattice has the 3 fewest deformation-split components of the candidate structures and generally the highest multiplicity component of a reflection correspond to the measured position […]"[15] prior to the (440) reflections. For the current study, as the use of synchrotron radiation allows for both a higher intensity and a better resolution, it was chosen for measuring XRD patterns up to the (222) reflection, from *eight* nitrided AISI 316L samples. The samples were nitrided at different conditions of time and temperature, and consequently, showed different properties, such as nitrogen concentration and nitrided layer thickness. In this study it was used a photon energy of 6.5 keV, whose XRD patterns were fitted using Fewell's model. Moreover, to consider nitrogen concentration gradient across the nitrided layer, each γ_N peak was decomposed in a few subpeaks, following the proposal of Öztürk and Williamson[16].

2. Material and Methods

Details of the preparation of the samples, which were plasma nitrided using 80% H_2-20% N_2, at 6 Torr, for 3 and 5 h using different temperatures (350, 400 and 450 °C), have been given previously[17], and the nitrided layer thickness (**t**) values are presented in Table 1. Here results for samples nitrided for 4h, using 400 and 450 °C are presented as well.

The phases formed on the nitrided samples were characterized by XRD, performed at the Brazilian Synchrotron Light Laboratory (LNLS), using synchrotron radiation (λ = 1.9074 Å or E = 6.5001 keV). The conditions were: θ-2θ geometry, at 0.2° steps, ranging from 47° ≤ 2θ ≤ 135°. A pyrolytic graphite analyzer and scintillation counter were used to obtain high signal to background with medium resolution.

In addition to the austenitic matrix and γ_N phase, the hexagonal ε ($Fe_{2-3}N$) was used in the XRD pattern fittings and, when necessary, cubic γ'(Fe_4N) and trigonal Cr_2N phases were used as well. The Le Bail technique was used to index the diffraction peaks in the experimental data[18,19], which were fitted using GSAS software[20] and EXPGUI graphical interface[21].

For the γ_N phase, having special triclinic symmetry[10,15], which presents a slight distortion (η) from fcc austenitic substrate structure was used. Based on the results of Öztürk and Williamson[16], we concluded that the best model to adopt in γ_N phase fittings was to consider it as a solid solution with a sequence of layers showing different contents of nitrogen. Each layer corresponds to a different lattice parameter $a\gamma_N$. The values for nitrogen concentration in each solid γ_N phases, $\mathbf{C_N}$, were calculated using Picard's equation[22]

$$a\gamma_N = a\gamma + \alpha\, C_N \qquad (1)$$

where α is a constant. The literature indicates a range of values for this constant, which depends on the $\mathbf{C_N}$ value[16]. The most commonly used (α = 0.0078 Å/at.% N) is known as Vegard´s constant[14,23]. Instead of this value, a different value is indicated, because the last one is used for low nitrogen concentrations (0-10 at.%). The new value is[16,24], α = 0.00861 Å/at.% N, which was adopted in this work.

3. Results and Discussion

Figure 1a presents the measured XRD patterns. The vertical bars show the positions of the fcc austenite peaks, labeled γ(hkl). All the XRD patterns show the expanded austenitic γ_N peaks, which are broader and shifted to lower diffraction angles, when compared to the correspondent austenite peaks. Figure 1b presents the penetration depth (**d**) of the synchrotron radiation.

The diffraction patterns presented in Figure 1 show a positive correlation between this penetration depth (**d**) of radiation and the nitrided layer thicknesses (**t**) (Table 1).

The γ (111) reflection whose **d** value (10.4 µm) is minimum, is observed for 350 and 400 °C, whose thickness is **t**< 10.4 µm. Moreover, the γ(111) intensity decreases when **t** increases, and is significantly higher than that of γ_N(111) for 350 °C, 3h, whose **t**=0.7 µm. The intensity decreases substantially at 400 °C (2.9 ≤ **t** ≤ 3.9 µm) and practically disappears at 450 °C, with 7.6 ≤ **t** ≤ 11µm, i.e., **t~d**. On the other hand, if we analyze the reflections of higher order, i.e., (311), where **d**~20 mm, the γ(311) intensity is comparable for 350 and 400 °C, which show **t** < **d**/7, but diminishes considerably at 450 °C, showing **t~d**/2.

Figure 2 shows the fitted diffraction lines (in red) on data points (black circles) for the samples nitrided for 3h. In order to see details of all the reflections on the XRD patterns, Figures 3a, b and c present a zoomed image from the region between 80° and 135° of Figure 2, showing all the phases which were used in the fittings. This region was selected because of the significative separation of the different γ_N phases, which is not observed in (111) and (200) reflections. Figure 4 illustrates details of the subpeaks, which were used for considering nitrogen concentration gradient across the nitrided layer.

3.1 Samples nitrided at 350 °C

Whereas *three* different γ_N phases were used in fittings for the samples nitrided for 3h, *four* phases were used for 5h sample. The austenite (a_γ = 3.597 Å) and the ε phases were used as well. The fitted values for the γ_N phases are presented in Table 2.

3.2 Samples nitrided at 400 °C

Four different γ_N phases were used in the fittings for the samples nitrided for 3h, while five phases were used for 4 and 5h samples. The austenite (a_γ = 3.597 Å) and the ε phases were used, as well as for 350 °C. In Table 3 are presented the fitted values for the γ_N phases.

For both temperatures, an additional phase appears for 5h, compared to 3h. This phase represents 25% (or 1/4) and 20% (or 1/5) of the total number used for γ_N subphases, for 350 and 400 °C, respectively. This rise can be explained by the increase of 23% and 21% (from 3 to 5h, for 350 and 400 °C, respectively) of nitrided layer thicknesses (**t**). This is because all the diffusion layers (and even the matrix) are certainly observed, as the x-ray penetration depth (**d**) complies with the equation 3.0t ≤ d≤ 27t. In this equation, the minimum corresponds to (111) reflection, for 400 °C, 5h and the maximum, to (222), for 350 °C, 3h. Moreover, as this additional phase presents lower N concentrations, it is located in the innermost layer, which is known as the diffusion layer.

Table 1. Thickness (**t**) of the samples' nitrided layers[17].

Temperature (°C)	**350**		**400**			**450**		
Time (h)	3	5	3	4	5	3	4	5
t (µm)	0.77±0.04	1.0±0.1	2.9±0.4	3.9±0.4	3.5±0.4	7.6±0.2	10±1	11±1

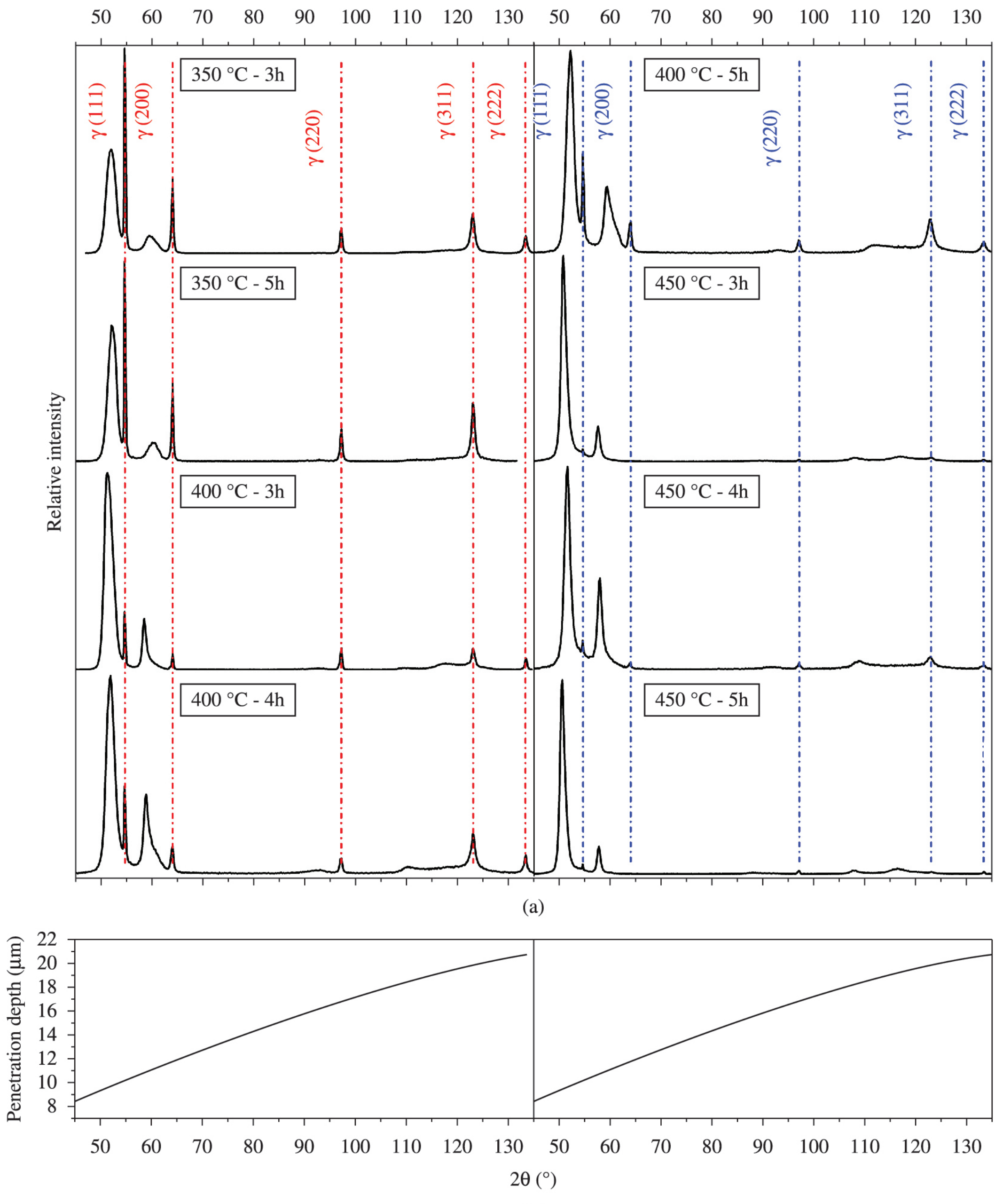

Figure 1. (a) X-ray diffraction patterns of the samples nitrided at different temperatures and times and (b) Synchrotron radiation (6.5keV) penetration depth (**d**) as a function of the diffracted angle.

3.3 Samples nitrided at 450 °C

Four different γ_N phases were used in the fittings for the samples nitrided for all times: 3, 4 and 5h. In addition to the austenite (a_γ = 3.597 Å), ε and γ' phases, the Cr_2N phase was used as well. Table 4 presents the fitted values for the γ_N phases.

These samples differ from the 350 and 400 °C samples in at least two different aspects. The first one is the same number of γ_N phases used in the fittings, for all times: 3, 4 and 5h. The second one is the γ_N phase concentration, whose minimum value is 31 at.%. For these samples, the interval that correlates **t** and **d** is 0.95t ≤ d≤ 2.7t; consequently, the observation of the diffusion layer may be much more difficult. Another possible and more likely explanation is that the diffusion layer might be less significant, relatively to 350 and 400 °C, as it decreases with the increasing the temperature, according to some authors[25,26].

It can be seen from the data in Tables 2 and 4 that while $\mathbf{C}_N \leq 30$ at.%, for 350 °C samples, $\mathbf{C}_N \geq 31$ at.% for 450 °C samples. It is likely that this behavior is related with the magnetic character of the γ_N phase, since it is known that

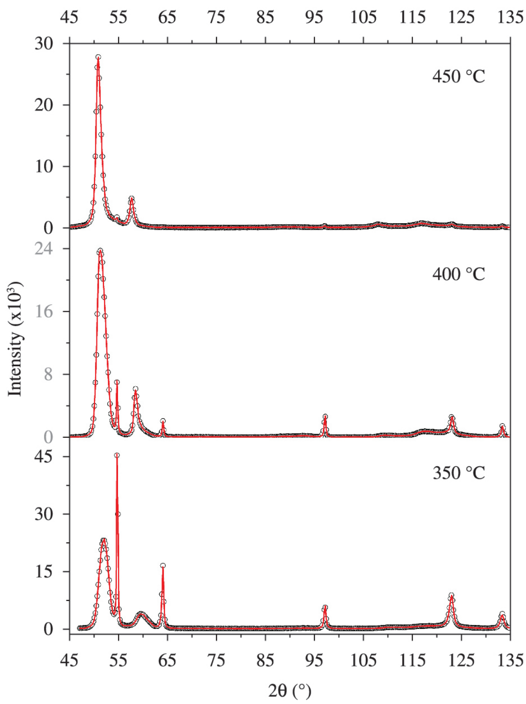

Figure 2. Fitted X-ray diffraction patterns for the samples nitrided for 3h at different temperatures.

this phase is paramagnetic (or magnetic) when its $\mathbf{C_N}$ is low (high)[16]. The Mössbauer Spectroscopy can show this behavior, and the results for all the samples will be presented in a future publication. If this is assumed, it is interesting to show that the lattice distortion η behavior in relation to $\mathbf{C_N}$ depends on the magnetic character of the respective γ_N phase. To evidence this aspect, Figure 5 shows η values as a function of $\mathbf{C_N}$ values, i.e., the fourth column as a function of the last column of Tables 2, 3 and 4.

This figure presents two very distinct regions: $\mathbf{C_N} \leq 30$ at.% (which is marked in a vertical dotted line), showing η ≤ 1.4° (in a horizontal dotted line, below) and the second one, indicating $\mathbf{C_N} \geq 31$ at.% and η ≥ 2.4° (in a horizontal dotted line, above), where the samples nitrided at 350 and 450 °C, respectively, can be observed and each one shows a typical behavior.

The paramagnetic γ_N phases in layers nitrided at 350 °C, for 3 and 5h, are very similar, showing a very high $\mathbf{C_N}$ gradient (approximately 60 at.%) between the inner region and the surface. At the same time, the lattice distortion η increases when $\mathbf{C_N}$ increases, and therefore it is higher near the surface, showing a slight variation, approximately 0.8°. On the other hand, the magnetic layers nitrided at 450 °C show a very different behavior: while the $\mathbf{C_N}$ gradient between the inner region and the surface is much smaller, showing a 20 to 30 at.% variation, the lattice

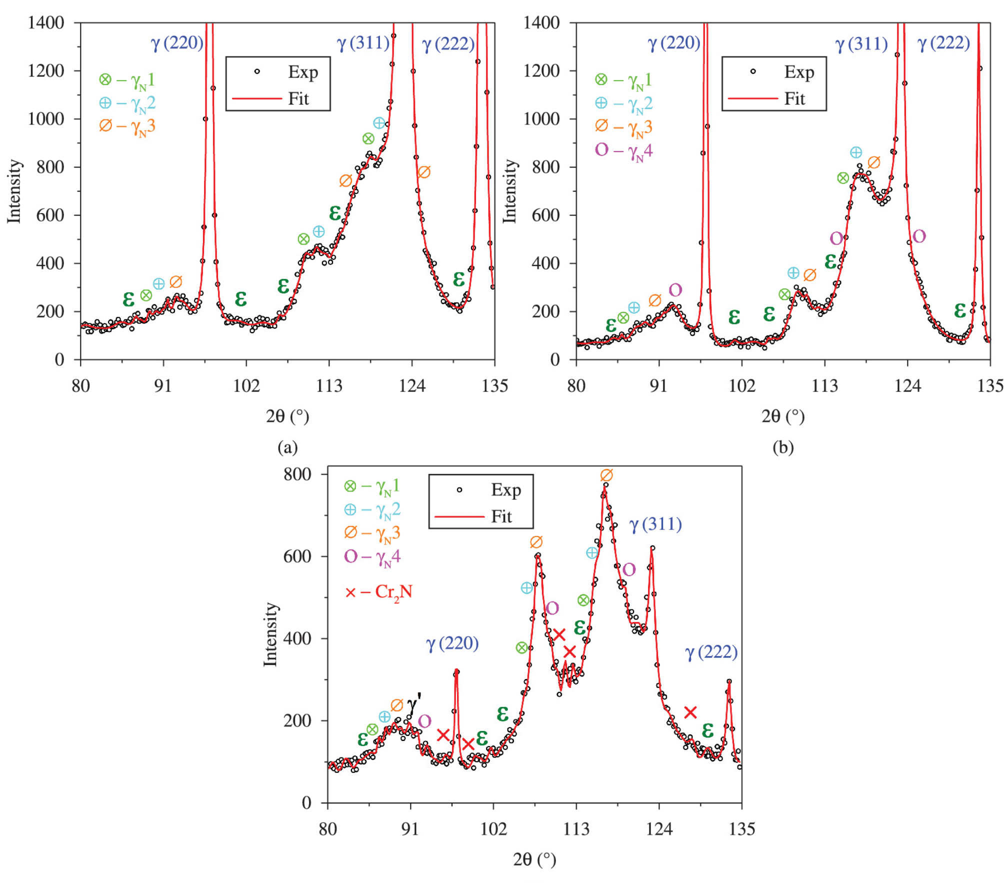

Figure 3. Zoom of the region between (220) and (222) reflections of Figure 3, for (a) 350, (b) 400 and (c) 450 °C.

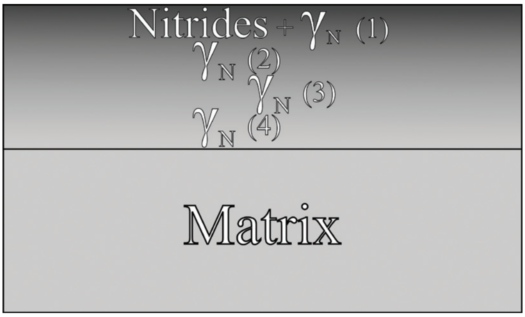

Figure 4. Illustration of the subpeaks used for the γ_N fittings.

Table 2. Values for Lattice parameter (**a**), Distortion (η) and Nitrogen concentration ($\mathbf{C_N}$) for each sublayer of the γ_N phases used in DRX pattern fittings for samples nitrided at 350 °C.

γ_N		$\mathbf{a_{\gamma N}}$ **(±0.01) Å**	**η (±0.1)°**	$\mathbf{C_N}$ **(± 3) at.%**
350 °C 3h	1	3.86	1.4	30
	2	3.80	1.2	23
	3	3.74	0.6	16
350 °C 5h	1	3.85	1.3	29
	2	3.82	1.3	26
	3	3.78	1.1	21
	4	3.74	0.6	16

Table 3. Values for Lattice parameter (**a**), Distortion (η) and Nitrogen concentration ($\mathbf{C_N}$) for each sublayer of the γ_N phases used in DRX pattern fittings for samples nitrided at 400 °C.

γ_N		$\mathbf{a_{\gamma N}}$ **(±0.01) Å**	**η (±0.1)°**	$\mathbf{C_N}$ **(± 3) at.%**
400 °C 3h	1	3.92	2.2	37
	2	3.91	3.0	36
	3	3.87	2.9	31
	4	3.77	1.3	20
400 °C 4h	1	3.90	2.3	35
	2	3.89	3.1	34
	3	3.80	2.7	23
	4	3.74	1.1	16
	5	3.70	1.2	12
400 °C 5h	1	3.87	2.8	31
	2	3.84	2.7	28
	3	3.77	1.5	20
	4	3.74	1.6	16
	5	3.71	1.8	13

distortion η, which is maximum in the inner region, shows a variation between 1.3° and 2.4° for 5 and 3h, respectively. For 4h, while $\mathbf{C_N}$ shows the highest interval, between 31 and 43 at.%, η shows a very smooth variation of 0.7°. Moreover, Williamson and Öztürk[16] suggested that the magnetic γ_N phase is analogous to the fcc ordered γ'-Fe_4N, which has a more expanded fcc lattice compared with γ-Fe and is ferromagnetic at room temperature. In this respect, our results seem to agree with their suggestion, because lattice distortion η decreases when $\mathbf{C_N}$ increases, near the

Table 4. Values for Lattice parameter (**a**), Distortion (η) and Nitrogen concentration ($\mathbf{C_N}$) for each sublayer of the γ_N phases used in DRX pattern fittings for samples nitrided at 450 °C.

γ_N		$\mathbf{a_{\gamma N}}$ **(±0.01) Å**	**η (±0.1)°**	$\mathbf{C_N}$ **(± 3) at.%**
450 °C 3h	1	3.98	3.2	44
	2	3.96	3.8	42
	3	3.94	4.9	39
	4	3.91	5.6	36
450 °C 4h	1	3.97	4.1	43
	2	3.95	4.4	41
	3	3.92	4.8	37
	4	3.87	4.9	31
450 °C 5h	1	3.96	2.4	42
	2	3.95	2.5	41
	3	3.92	2.9	37
	4	3.87	3.7	31

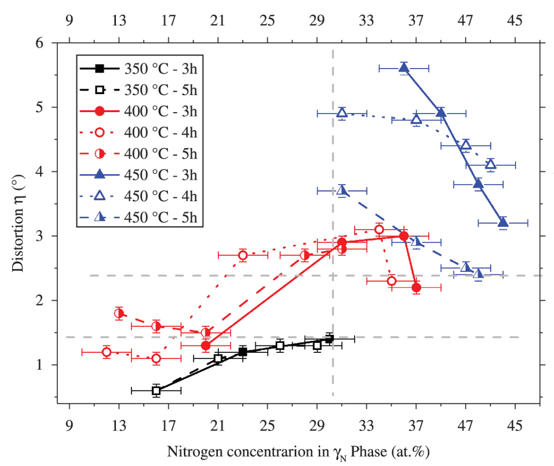

Figure 5. Lattice distortion as a function of nitrogen concentration for each sublayer of the γ_N phases used in DRX patterns fittings, for all the nitrided samples.

surface, for 450 °C samples, indicating a higher symmetry for the subphase which is more magnetic. Therefore, our assumption seems to be correct.

Regarding the samples nitrided at 400 °C, they show magnetism and paramagnetism simultaneously[9], and are magnetic near the surface and paramagnetic in the inner region, which can be observed in Figure 5. This figure indicates that the behavior of these samples is not uniform as is for the samples nitrided at 350 and 450 °C. However, the γ_N phases presenting $\mathbf{C_N}$ in the same interval observed for 350 °C samples, i.e., for $17 \leq \mathbf{C_N} \leq 30$ at.%, show the same behavior observed for these samples. In other words, the lattice distortion η increases when $\mathbf{C_N}$ increases, although it increases to 3.0°, which is significantly higher than the value observed for the 350 °C samples, i.e., 1.4°. On the other hand, for $\mathbf{C_N} \geq 31$ at.%, for both 3 and 4h, for the most superficial layer, η decreases to a value very close to 2.4°, which is the η reference value for the samples nitrided at 450 °C.

4. Conclusion

1) Regarding γ_N phases magnetic character, our results indicate that magnetic behavior, observed for the samples nitrided at 450 °C, seems to be correlated not only with high nitrogen concentration ($\mathbf{C_N} \geq 31$ at.%), but also with high lattice distortion ($\eta \geq 2.4°$), which reached up to 5.6°. Moreover, this distortion decreases when $\mathbf{C_N}$ increases, consequently it has a minimum value at the surface.
2) On the other hand, for paramagnetic samples, nitrided at 350 °C, the lattice distortion η increases when $\mathbf{C_N}$ increases, up to 1.4° and 30 at.%, respectively. In this case, it has a maximum at the surface.
3) As the sample set showed a big range of layer thickness, this property was correlated to X-ray depths penetration from different reflections of XRD patterns, showing significant positive correlation between both.

Acknowledgements

This work was partly supported by the Brazilian research funding agencies FAPESP and CAPES. We gratefully acknowledge the National Laboratory of Light Synchrotron – LNLS, Brazil Grant No. XDR1/9101.

References

1. Williamson DL, Öztürk O, Wei R and Wilbur PJ. Metastable phase formation and enhanced diffusion in f.c.c. alloys under high dose, high flux nitrogen implantation at high and low ion energies. *Surface and Coatings Technology*. 1994; 65(1-3):15-23. http://dx.doi.org/10.1016/S0257-8972(94)80003-0.
2. Menthe E, Bulak A, Olfe J, Zimmermann A and Rie K-T. Improvement of the mechanical properties of austenitic stainless steel after plasma nitriding. *Surface and Coatings Technology*. 2000; 133-134:259-263. http://dx.doi.org/10.1016/S0257-8972(00)00930-0.
3. Liang W. Surface modification of AISI 304 austenitic stainless steel by plasma nitriding. *Applied Surface Science*. 2003; 211(1-4):308-314. http://dx.doi.org/10.1016/S0169-4332(03)00260-5.
4. Li G, Peng Q, Li C, Wang Y, Gao J, Chen S, et al. Effect of DC plasma nitriding temperature on microstructure and dry-sliding wear properties of 316L stainless steel. *Surface and Coatings Technology*. 2008; 202(12):2749-2754. http://dx.doi.org/10.1016/j.surfcoat.2007.10.002.
5. Xi Y, Liu D and Han D. Improvement of corrosion and wear resistances of AISI 420 martensitic stainless steel using plasma nitriding at low temperature. *Surface and Coatings Technology*. 2008; 202(12):2577-2583. http://dx.doi.org/10.1016/j.surfcoat.2007.09.036.
6. Olzon-Dionysio M, de Souza SD, Basso RLO and de Souza S. Application of Mössbauer spectroscopy to the study of corrosion resistance in NaCl solution of plasma nitrided AISI 316L stainless steel. *Surface and Coatings Technology*. 2008; 202(15):3607-3614. http://dx.doi.org/10.1016/j.surfcoat.2007.12.040.
7. Fossati A, Borgioli F, Galvanetto E and Bacci T. Corrosion resistance properties of glow-discharge nitrided AISI 316L austenitic stainless steel in NaCl solutions. *Corrosion Science*. 2006; 48(6):1513-1527. http://dx.doi.org/10.1016/j.corsci.2005.06.006.
8. Li CX and Bell T. Corrosion properties of active screen plasma nitrided 316 austenitic stainless steel. *Corrosion Science*. 2004; 46(6):1527-1547. http://dx.doi.org/10.1016/j.corsci.2003.09.015.
9. Campos M, de Souza SD, de Souza S and Olzon-Dionysio M. Improving the empirical model for plasma nitrided AISI 316L corrosion resistance based on Mössbauer spectroscopy. *Hyperfine Interactions*. 2011; 203(1-3):105-112. http://dx.doi.org/10.1007/s10751-011-0351-3.
10. Fewell MP, Mitchell DRG, Priest JM, Short KT and Collins GA. The nature of expanded austenite. *Surface and Coatings Technology*. 2000; 131(1-3):300-306. http://dx.doi.org/10.1016/S0257-8972(00)00804-5.
11. Blawert C, Mordike BL, Jirásková Y and Schneeweiss O. Structure and composition of expanded austenite produced by nitrogen plasma immersion ion implantation of stainless steels X6CrNiTi1810 and X2CrNiMoN2253. *Surface and Coatings Technology*. 1999; 116-119:189-198. http://dx.doi.org/10.1016/S0257-8972(99)00086-9.
12. Blawert C, Kalvelage H, Mordike BL, Collins GA, Short KT, Jirásková Y, et al. Nitrogen and carbon expanded austenite produced by PI3. *Surface and Coatings Technology*. 2001; 136(1-3):181-187. http://dx.doi.org/10.1016/S0257-8972(00)01050-1.
13. Gontijo LC, Machado R, Miola EJ, Casteletti LC, Alcântara NG and Nascente PAP. Study of the S phase formed on plasma-nitrided AISI 316L stainless steel. *Materials Science and Engineering A*. 2006; 431(1-2):315-321. http://dx.doi.org/10.1016/j.msea.2006.06.023.
14. Mingolo N, Tschiptschin AP and Pinedo CE. On the formation of expanded austenite during plasma nitriding of an AISI 316L austenitic stainless steel. *Surface and Coatings Technology*. 2006; 201(7):4215-4218. http://dx.doi.org/10.1016/j.surfcoat.2006.08.060.
15. Fewell MP and Priest JM. High-order diffractometry of expanded austenite using synchrotron radiation. *Surface and Coatings Technology*. 2008; 202(9):1802-1815. http://dx.doi.org/10.1016/j.surfcoat.2007.07.062.
16. Öztürk O and Williamson DL. Phase and composition depth distribution analyses of low energy, high flux N implanted stainless steel. *Journal of Applied Physics*. 1995; 77(8):3839-3850. http://dx.doi.org/10.1063/1.358561.
17. Olzon-Dionysio M, Campos M, Higa OZ, Cunha TF and Souza SD. Investigating the correlation between some of the properties of plasma nitrided AISI 316L stainless steel. *Materials Research*. 2013; 16(5):1052-1057. http://dx.doi.org/10.1590/S1516-14392013005000081.
18. Le Bail A, Duroy H and Fourquet JL. Ab-initio structure determination of LiSbWO6 by X-ray powder diffraction. *Materials Research Bulletin*. 1988; 23(3):447-452. http://dx.doi.org/10.1016/0025-5408(88)90019-0.
19. Le Bail A. Whole powder pattern decomposition methods and applications: A retrospection. *Powder Diffraction*. 2005; 20(4):316-326. http://dx.doi.org/10.1154/1.2135315.
20. Larson AC and Von Dreele RB. *General Structure Analysis System (GSAS)*. Los Alamos: Los Alamos National Laboratory; 2004. Los Alamos National Laboratory Report, LAUR-86-748.

21. Toby BH. EXPGUI, a graphical user interface for GSAS. *Journal of Applied Crystallography*. 2001; 34(2):210-213. http://dx.doi.org/10.1107/S0021889801002242.
22. Picard S, Memet JB, Sabot R, Grosseau-Poussard JL, Rivière JP and Meilland R. Corrosion behaviour, microhardness and surface characterisation of low energy, high current ion implanted austenitic stainless steel. *Materials Science and Engineering A*. 2001; 303(1-2):163-172. http://dx.doi.org/10.1016/S0921-5093(00)01841-4.
23. Jack DH and Jack KH. Invited review: Carbides and nitrides in steel. *Materials Science and Engineering*. 1973; 11(1):1-27. http://dx.doi.org/10.1016/0025-5416(73)90055-4.
24. Ledbetter HM and Austin MW. Dilation of an fcc Fe–Cr–Ni alloy by interstitial carbon and nitrogen. *Materials Science and Technology*. 1987; 3(2):101-104. http://dx.doi.org/10.1179/mst.1987.3.2.101.
25. Borgioli F, Fossati A, Galvanetto E and Bacci T. Glow-discharge nitriding of AISI 316L austenitic stainless steel: influence of treatment temperature. *Surface and Coatings Technology*. 2005; 200(7):2474-2480. http://dx.doi.org/10.1016/j.surfcoat.2004.07.110.
26. Li Y, Wang L, Xu J and Zhang D. Plasma nitriding of AISI 316L austenitic stainless steels at anodic potential. *Surface and Coatings Technology*. 2012; 206(8-9):2430-2437. http://dx.doi.org/10.1016/j.surfcoat.2011.10.045.